Force-dependent remodeling of a tight junction protein ZO-1 is regulated by phase separation

Noriyuki Kinoshita*[1,3], Takamasa S. Yamamoto[1], Naoko Yasue[1], Toshihiko Fujimori[2,3], and Naoto Ueno*[1,3,4]

1: Division of Morphogenesis, Department of Developmental Biology, National Institute for Basic Biology, 38 Nishigonaka, Myodaiji, Okazaki, Aichi, 444-8585, Japan.

2: Division of Embryogenesis, Department of Developmental Biology, National Institute for Basic Biology, 5-1 Higashiyama, Myodaiji, Okazaki, Aichi 444-8787, Japan

3: School of Life Science, SOKENDAI (The Graduate University for Advanced Studies), Okazaki, Aichi, 444-8585, Japan

4: Lead Contact

* corresponding authors:
nueno@nibb.ac.jp (N.U.), nkinoshi@nibb.ac.jp (N.K.)

Summary

Although the physiological importance of biomolecular condensates is widely recognized, how it is controlled in time and space during development is largely unknown. Here we show that a tight junction protein ZO-1 forms cytoplasmic condensates in the trophectoderm (TE) of the mouse embryo before E4.0. These disappear via dissolution, and ZO-1 accumulates at the cell junction as the blastocyst cavity grows, and internal pressure on TE cells increases. In contrast, the dissolution is less evident in TE cells attached to the inner cell mass, as they receive weaker tensile forces. Furthermore, analyses using MDCK cells have shown that the ZO-1 condensates are generated and maintained by liquid-liquid phase separation. Our study also highlights that the dynamics of these condensates depends on the physical environment via the interaction between ZO-1 and F-actin. We propose that the force-dependent regulation of ZO-1 condensation contributes to establishing robust cell-cell adhesion during early development.

Keywords

Cell-to-cell adhesion, ZO-1, tight junction, mechanical force, mouse development, condensate, liquid-liquid phase separation (LLPS), intrinsically disordered region (IDR).

Introduction

Mechanical forces are generated at different times and in different tissues during the development of organisms, due to the dynamic movement and shape change of cells and tissues (Bodor et al., 2020), growth of a cell mass by proliferation (Godard and Heisenberg, 2019), the removal of cells by apoptosis (Teng et al., 2017), luminal pressure (Chan et al., 2019), and shear stress of body fluids such as blood (Paolini and Abdelilah-Seyfried, 2018), etc. All of these forces can contribute to the morphogenesis of organs through mechanochemical feedback mechanisms (Hannezo and Heisenberg, 2019). Although the presence and physiological importance of such forces have long been implicated in the homeostasis as well as morphogenesis of living organisms (Hallou and Brunet, 2020; Thompson, 1917), how cells sense and respond to these forces are not fully understood at the molecular level. In this study, we demonstrate that the remodeling of ZO-1 through the regulation of liquid-liquid phase separation (LLPS) is mechanically controlled.

In our previous study using *Xenopus laevis* embryos, we demonstrated that among a number of identified phosphoproteins, cell junction- as well as focal adhesion-related proteins are highly phosphorylated immediately after the application of mechanical forces by centrifugation or compression (Hashimoto et al., 2019). Intriguingly, a global analysis of the phosphoproteome suggested that the mechanical stimuli induced the embryonic cells to adopt an epithelial state rather than a mesenchymal state, known as the mesenchymal-epithelial transition (MET), which is opposite to the epithelial-mesenchymal transition (EMT), a well-characterized phenomenon in some developmental contexts and in cancer pathogenesis in which cells compromise their cell-to-cell adhesiveness (Baum et al., 2008). In fact, we confirmed that adherens- and tight junction, revealed by the accumulation of C-cadherin (Choi et al., 1990; Ginsberg et al., 1991) and ZO-1 (Anderson et al., 1988), respectively, became enhanced after the application of force. We also found that F-actin, which is normally localized in the basal and lateral domain of cells, accumulated at the apical domain, reinforcing the stiffness of the cell cortex (Hashimoto et al., 2019). These observations suggest that these junctions were remodeled following the force stimuli and that the cells adopted more epithelialized states. This led us to propose that force-induced epithelialization is an important cellular response to physical forces to maintain the integrity of a tissue, allowing it to acquire robustness against forces which might perturb normal morphogenesis.

More recently, we showed that FGFR1 is activated, and that Erk2 is consequently phosphorylated and translocated into the nucleus in ectodermal cells (Kinoshita et al., 2020) to achieve MET during gastrulation. During the course of that study, we repeatedly observed that ZO-1 condensates were found as puncta in ectoderm cells prior to, but not after, gastrulation (Kinoshita et al., 2020). Based on previous reports that showed that ZO-1 can undergo LLPS in zebrafish embryos (Schwayer et al., 2019) and cultured cells (Beutel et al., 2019), we speculated that the ZO-1 LLPS is mechanically regulated, particularly by dynamic morphogenesis known as epiboly during gastrulation which imposes a tensile force on the ectoderm (Hernandez-Vega et al., 2017).

To extend the above study that employed *Xenopus laevis*, and to examine whether our working model could be extrapolated to other species such as mammals, we focused on mouse embryogenesis in this study. Basically, we obtained similar results to those with *Xenopus* and found that cytoplasmic condensates of ZO-1 exist in the trophectoderm (TE) cells of early mouse embryos before E4.0, although the condensate disappears upon stretching of TE cells due to the expansion of the blastocyst cavity (blastocoel).

To confirm that ZO-1 condensates are the product of cellular LLPS, a physical process to facilitate the demixing of proteins through protein condensation (Brangwynne, 2013), we used on cultured cells in which condensates of GFP-ZO-1 were observed in various conditions. Following both the treatment of a cell-permeabilizing agent digitonin (Shiina, 2019), and analyses with fluorescent recovery after photobleaching (FRAP), ZO-1 condensates have been shown to have typical properties of liquid droplets generated by LLPS. We also identified that the N-terminal fragment of ZO-1, which contains intrinsically disordered regions (IDRs) (Kato et al., 2012; Li et al., 2012), an unstructured stretch of an amino acid sequence of low complexity, are sufficient for phase separation of ZO-1. Finally, we highlighted the importance of cytoskeletal actin in the regulation of ZO-1 assembly and propose that ZO-1 protein became liberated from the droplets and was deployed to enhance the tight junction in a force-dependent manner. This was supported by observations of MDCK cells in different culture conditions, including wound healing.

The present study, which used early mouse embryos and cultured cells, reveals a previously unknown role of physical force that regulates the condensation of ZO-1 and contributes to the enhancement of cell-to-cell adhesion during early development.

Results

ZO-1 condensates in early mouse embryos

To examine whether the behavior of ZO-1 protein in *Xenopus laevis* embryos which we reported previously (Kinoshita et al., 2020) is conserved across species, especially in mammals, we first performed immunostaining of ZO-1. We focused on E3.5 and E4.5 embryos since they hatch out of the zona pellucida (ZP) and expand their shape (Figure 1A). We fixed E3.5 and E4.5 embryos with paraformaldehyde and immunostained with a ZO-1 antibody (Figure 1B). We found that the cells of E3.5 embryos showed a significantly higher number of ZO-1 puncta in the cytoplasm relative to E4.5 embryos. As development proceeded, the surface area of TE cells, particularly on the mural side, expanded (Figure 1E) and became thinner (data not shown). We found that the number of cytoplasmic ZO-1 puncta were reduced and ZO-1 signal intensity at the plasma membrane in E4.5 embryos became much higher than those of E3.5 embryos at the expense of its cytoplasmic pool (Figure 1C, D mural), without changing the total fluorescence intensity of the protein (Figure 1F left). Importantly, this change coincides well with the accumulation of F-actin at the cell cortex in E4.5 embryos (Figure 1B and 1F right). This result suggests that the shuttling of ZO-1 protein from the cytoplasmic puncta to cell junctions occurs as development progressed. We observed a similar behavior of ZO-1 protein using ZO-1-EGFP-expressing mouse embryos by live-imaging (Katsunuma et al., 2016) (Video S1 and Figure S1).

Interestingly, however, in the polar TE cells attached to the inner cell mass (ICM) of E4.5 embryos, a significant number of condensates remained in the cytoplasm (lower panels in Figure 1B lower and Figure 1D). Consistently, the fluorescence intensity of anti-ZO-1 immunostaining at the plasma membrane in the polar TE cells was lower than that in the mural cells (Figure 1G left). In addition, the accumulation of F-actin at the cell membrane was also more evident in mural cells, which expanded more than polar TE cells (Figure 1G right). Since polar TE cells attach to the crowded ICM, these cells may be exposed to lower tensions.

These results are consistent with our previous finding that ZO-1 condensates decrease in the *Xenopus* ectodermal cells exposed to a higher tensile force (Hashimoto et al., 2019; Kinoshita et al., 2020). Those findings suggest that the embryonic cells of E4.5 embryos, especially TE cells on which more potent tensile forces than those of E3.5 embryos are applied due to the inner pressure of the growing blastocyst cavity, might have reduced the

145 number and volume of ZO-1 puncta in the cytoplasm.
146
147 ***ZO-1 condensate is regulated by a force-dependent mechanism***
148 It is known that developing mouse embryos from E4.0 to E4.5 experience a gradually
149 increasing magnitude of luminal pressure due to expansion of the blastocyst cavity in the
150 presence of the ZP (Chan et al., 2019; Leonavicius et al., 2018). Accordingly, the cortical
151 tension of TE increases from E3.5 to E4.5 (Chan et al., 2019). To confirm that the
152 disappearance of ZO-1 condensates from the cytoplasm is dependent on a mechanical
153 force (inner hydraulic pressure of blastocyst cavity) , using ouabain, we inhibited Na^+/K^+
154 ATPase which promotes the influx of water and therefore increases the volume of the
155 blastocyst cavity (Figure 2A, B). In these ouabain-treated embryos, significant numbers
156 of ZO-1 condensates were retained in the cytoplasm of the mural cells of E4.5 embryos
157 (Figures 2C-E), demonstrating that the cells released from the tension failed to trigger the
158 dissolution of the ZO-1 condensates.
159 Next, we mechanically reduced tension by releasing the blastocoel fluid of the ZO-1-
160 EGFP-expressing embryos by piercing embryos with a glass needle. Immediately after
161 they were pierced, embryos shrank and membrane localization of ZO-1 was reduced,
162 although it recovered within several hours (Figure 2F, G and Video S2). Immunostaining
163 with the anti-ZO-1 antibody confirmed that endogenous ZO-1 also behaves in a similar
164 way, observing more cytoplasmic puncta in pierced E4.5 embryos than in control E4.5
165 embryos (Figure S2). Together, these results suggest that ZO-1 condensate deforms in a
166 tensile force-dependent manner.
167
168 ***Cell type-dependent condensation of ZO-1***
169 To investigate the nature of the ZO-1 condensate, we performed a series of studies using
170 *Xenopus laevis* A6 cells in which full-length and mutant forms of GFP-ZO-1 were
171 transiently expressed for live-imaging (Figure 3A). In non-confluent A6 cells, full-length
172 GFP-ZO-1 localized mostly in the cell periphery and partially colocalized with F-actin
173 bundles (Figure 3B). It was intriguing, however, that in A6 cells, when GFP-ZO-1, which
174 lacks an actin-binding domain (Fanning et al., 2002) (GFP-ZO-1ΔABD), was expressed,
175 ZO-1 condensates became evident and formed large droplet-like structures with a smooth
176 surface (Figure 3C). This suggests that the formation of condensate is normally restricted
177 by the binding of ZO-1 to F-actin (Beutel et al., 2019; Schwayer et al., 2019) and that

178 GFP-ZO-1ΔABD lost its capacity for the interaction. In addition, we expressed the N-
179 terminal half and the C-terminal half of ZO-1 tagged with GFP (Figure 3A; GFP-ZO-1ΔC
180 and ΔN, respectively). Of note, the N-terminal half contains two IDRs while the C-
181 terminal half has one relatively long stretch of IDR. We found that the N-terminal half is
182 sufficient to form condensates in the cytoplasm (Figure 3D).
183 Supporting this notion, co-expression with a red fluorescent protein fused to F-actin-
184 binding peptides, Lifeact, Utrophin and the actin-binding domain of Moesin
185 (MoesinABD) similarly induced condensates that were indistinguishable from those
186 induced by GFP-ZO-1ΔABD (Figure 3E). We also observed that the MoesinABD-
187 induced ZO-1 condensates dynamically moved, sometimes fused and underwent fission
188 (Video S3 and Figure S3), reminiscent of typical liquid droplets. Based on these results,
189 we speculate that the interaction of ZO-1 with F-actin might block the formation of large
190 condensates. We thus treated cells with Latrunculin B, a potent inhibitor of actin
191 polymerization, and found that the formation and extinction of cytoplasmic ZO-1
192 condensates depended on the development and destruction of the F-actin network (Figure
193 3F and Video S4). These observations clearly indicate that the efficiency and growth of
194 ZO-1 condensation are negatively regulated by the interaction with F-actin in A6 cells.
195 We next expressed GFP-ZO-1 in canine MDCK cells, which formed an epithelial-like
196 cell sheet when they reached confluence. In sharp contrast to A6 cells, naïve MDCK cells
197 in a non-confluent sparse culture displayed evident condensates in the cytoplasm (Figure
198 4A). The average size of the ZO-1 condensate in A6 cells co-expressing MoesinABD and
199 the naïve MDCK cells visualized by immunostaining were 0.8 μm and 0.7 μm,
200 respectively (Figure 4B). These observations indicate that the condensation and
201 localization of ZO-1 proteins depend largely on cell type. We then analyzed the properties
202 of ZO-1 condensates in these cells.
203
204 ***Dynamics of ZO-1 condensation in cultured cells***
205 To examine whether the ZO-1 condensates observed in the cultured cells are indeed the
206 products of LLPS, we first treated A6 cells harboring GFP-ZO-1 puncta by co-expressing
207 MoesinABD with digitonin, a cell-permeabilizing reagent that disrupts the equilibrium
208 between the condensate and the cytoplasm. That treatment shrank the condensates within
209 several minutes in A6 cells (Figure 4C and Video S5). GFP-ZO-1 puncta in MDCK cells
210 behaved in a similar way following digitonin treatment (Figure 4D and Video S6).

211 Furthermore, we performed FRAP analyses for the condensates in A6 cells expressing
212 MoesinABD or in naïve MDCK cells. In both A6 (+MoesinABD) and MDCK cells, after
213 photo-bleaching, fluorescence immediately started to recover, reaching approx. 50%
214 (Figure 4E and F). This quick and high recovery is a typical property of LLPS-mediated
215 condensates (Shiina, 2019). These results demonstrate that the ZO-1 puncta are droplet-
216 like condensates produced by LLPS and in equilibrium with the cytoplasm.
217
218 ***Disassembly of ZO-1 condensate is regulated by the establishment of robust cell-to-cell***
219 ***contact***
220 To test the possibility that the formation of ZO-1 condensate is influenced by the
221 mechanical environment in cultured cells as predicted from mouse embryogenesis, we
222 grew MDCK cells to form islands in a culture dish. In those islands, cells in the central
223 region reached confluence and formed a typical epithelial cell sheet. When we examined
224 the condensate formation in the confluent MDCK monolayer, it was notable that cells in
225 the central region lost the condensates, while the peripheral cells tended to have well-
226 grown condensates (Figure 5A and B). However, we occasionally observed cells that
227 harbor relatively large-sized condensates in the central region, but those cells were not
228 well attached to, and were free from, neighboring cells (data not shown). A similar
229 tendency was observed for endogenous ZO-1 protein detected by immunofluorescence
230 using the anti-ZO-1 antibody (Figure 5C). As shown in the graph, cells in the forefront
231 row (most outer layer) and the second row had 15 to 20 condensates per cell on average,
232 whereas cells in the inner or central region had only a few condensates (Figure 5D). One
233 feature that distinguishes the inner cells from peripheral cells is that after the cells reach
234 confluency, the former adopt polygonal shapes and have higher densities than the latter
235 (Figure 5C). This suggests that the inner cells establish a robust cell-to-cell contact by
236 tight and adherens junctions which is physically supported by the actin cytoskeleton and
237 an individual cell rigidly contacts with surrounding cells, resembling embryonic cells
238 under tensile force.
239 To support this idea, we conducted a laser ablation assay. MDCK cells were grown so
240 that the cells formed islands in one culture dish. Then the GFP-ZO-1 expression plasmid
241 was transfected and the plasma membrane of GFP-ZO-1–expressing cells was irradiated
242 with laser light. When cells inside of colonies that had ZO-1 at the cell junction were
243 irradiated, cells became stable after irradiation due to cell-cell contact with neighboring

cells (Figure 5E and Video S7). When peripherally-located cells which had ZO-1 puncta were irradiated, those cells immediately erupted and disappeared after irradiation (Figure 5F and Video S8). These results suggest that in MDCK cells, the formation of ZO-1 condensate is negatively associated with the establishment of robust cell-to-cell contact.

To verify that idea, we reduced the cell-to-cell contact by treating MDCK cells expressing GFP-ZO-1 with PBS containing trypsin-EDTA. When the trypsin-EDTA solution was added, ZO-1 detached from the cell membrane and formed puncta as cells lost their contact (Figure S4 and Video S9). This result further confirmed the idea that the formation of ZO-1 condensate is regulated by cell-cell adhesion.

To further examine whether cell-to-cell contact negatively regulates ZO-1 condensate formation in MDCK cells, we conducted a wound-healing assay using GFP-ZO-1–expressing cells (Figure 6A-C and Video S10). Initially, most of the cells had few condensates in a confluent cell sheet. After scratching, cells started to actively move toward the wound site, forming a significant number of condensates. The FRAP assay revealed that the fluorescent signals of GFP-ZO-1 condensates that formed during the wound-healing assay recovered to about 40% within 10 min, suggesting that these condensates were formed by LLPS (Figure S5A-C, Video S11 and S12). This result indicates again that the formation of ZO-1 condensate is regulated by inter- and extracellular environments such as cell-to-cell contact, which in turn suggests that the cells that are harnessed with a well-developed F-actin network due to higher levels of cell-to-cell adhesion may hamper ZO-1 condensation. In fact, cortical F-actin was well-developed in the non-migrating polygonal cells far from the wound site, whereas migrating cells around the wound site developed more stress fibers at the expense of cortical actin (Figure 6D-F). This is consistent with our previous finding that *Xenopus* embryonic cells lost ZO-1 condensates when cell-to-cell junctions were enhanced after the application of force (Hashimoto et al., 2019; Kinoshita et al., 2020).

In addition, we found that hyper-osmolarity also induced the formation of ZO-1 condensate. When A6 cells expressing GFP-ZO-1 were treated with a high-salt medium, ZO-1 formed puncta (Figure S5D and Video S13). They reversibly recovered when the high-salt medium was washed out, indicating that ZO-1 LLPS is regulated by osmolarity. As increased extracellular osmolarity led to a reduction in cell volume and loosening of the cell membrane, this cellular phenotype may also be attributed to decreased membrane tension and remodeling of F-actin.

Discussion

Our present study using mouse embryos as well as cultured cells, together with a previous study with *Xenopus* embryos, indicate that similar mechanisms may govern cellular responses to force across species. Briefly, mechanical stresses induced by forces generated by dynamic morphogenesis and/or vigorous cell movements during development, such as gastrulation, activate the force-dependent pathway leading to the remodeling of cell-to-cell junctions. The present study also suggests that the process involves the negative regulation of LLPS of ZO-1, leading to the collapse of ZO-1 condensates in the cytoplasm. Since embryonic tissues, as well as some adult tissues such as heart and blood vessels, are constantly exposed to various forces including tensile force, shearing force, etc., and since ZO-1 is a structurally conserved protein among species, we propose that this mechanism may be employed to maintain the robustness and integrity of tissues against various forces in general, and could also be an evolutionary innovation when multicellular animal species such as placozoa emerged (Gonzalez-Mariscal et al., 2011). Although our previous study using *Xenopus* embryos identified that the function of the FGF receptor is essential for the force-induced pathway, it also suggested that FGF ligands are not required for signal activation, shedding light onto the as yet unrevealed activation mechanisms for FGFRs and other receptor tyrosine kinases (RTKs) by force. In fact, epidermal growth factor receptor (EGFR), which is an upstream RTK for Erk, was implicated in the mechanical force-dependent activation of Erk in the collective migration of wound-healing cells (Hino et al., 2020). In both cases, cell deformation by tensile forces appears to be the trigger of these pathways, supporting the idea that mechanoresponsive signaling pathways may be highly conserved.

Interestingly, our present study using cultured cells demonstrated that the efficacy of ZO-1 condensation as droplets largely depends on cell type, with MDCK cells forming droplets in standard culture conditions whereas A6 cells only did so when the actin-binding domain of ZO-1 was genetically deleted (ΔABD), actin-polymerization was inhibited, or actin was masked by its binding chemicals. These results suggest that the disintegration of ZO-1 condensates in the cytoplasm is regulated by the interaction between ZO-1 and F-actin, which in turn suggests that the difference between the amount and dynamics of F-actin may distinguish these two cell types. Conversely, the revelation of ZO-1 from F-actin is critical for maintaining large-sized ZO-1 condensate. These

310 notions further suggest that the control of ZO-1 re-localization from the cytoplasm to tight
311 junctions is dependent on the remodeling of cytoskeletal actin. At present, it is unclear
312 how the FGFR/Mek/Erk signal triggers or is related to the remodeling of actin and leads
313 to the accumulation of ZO-1 to the junction, but it is assumed that the signal is converted
314 into F-actin remodeling or ZO-1 phosphorylation, or both, as discussed next.
315 First, Erk might be able to regulate F-actin polymerization through small G proteins
316 such as GEF-H1 and its downstream target RhoA (Fujishiro et al., 2008; Itoh et al., 2014;
317 Ren et al., 1998). As described above, it was recently reported that Erk is activated in
318 collectively migrating MDCK cells by EGFR and regulates F-actin organization and
319 cellular contraction (Hino et al., 2020). Second, it is also possible that the cascade of
320 phosphorylation initiated by FGFR might eventually result in the phosphorylation of ZO-
321 1 protein, which has a number of potential phosphorylation sites for Ser/Thr kinases,
322 raising the possibility that phosphorylation of ZO-1 by Erk or other kinases may be a key
323 event for condensate dissolution. In fact, our previous report identified one particular site
324 in ZO-1 (Ser278) in the N-terminal half containing two putative IDRs that are sufficient
325 to form condensate, which was phosphorylated immediately after the application of force
326 and dephosphorylated within an hour (Hashimoto et al., 2019). Functional examination
327 of a possible link between RTK signaling and F-actin remodeling and a detailed
328 investigation of ZO-1 phosphorylation sites, which are sensitive to force and regulate
329 condensation, would provide useful information to clarify the force-dependent pathway.
330 What is the physiological significance of ZO-1 condensate formation? Why does ZO-1
331 need to be compartmentalized into the condensate? This may be too premature to discuss
332 before the nature of the ZO-1–containing condensate is fully understood, but we would
333 like to propose that the condensate serves as a reservoir for ZO-1 protein when cells are
334 relatively relaxed. Then, during development when the cells become stretched by tensile
335 force leading to the activation of Erk and the remodeling of F-actin, ZO-1 condensate
336 undergoes dissolution, and ZO-1 protein is delivered to the tight junction to exert its
337 function. It has been reported that tension mediates the remodeling of cell junctions (Ito
338 et al., 2017). Phase separation of ZO-1 may be directly involved in this regulatory system.
339 In this scenario, it is possible that LLPS acts as an on-demand ON/OFF switch of ZO-1
340 supply to the cell membrane from cytoplasm. This “reservoir mechanism” for ZO-1 may
341 be shared and employed by multicellular animal species and its evolutionary origin is an
342 intriguing problem worth studying in the future.

ZO-1, which is an essential component of the tight junction, contributes to establishing cell-to-cell adhesion and is therefore implicated in various pathologies, including cancer. Particularly, in EMT, the loss of cell-to-cell adhesion is known to drive the progress and metastasis of cancer. It is also known that in neuronal cells, some condensates which contain proteins such as the RNA-binding protein FUS (Murray et al., 2017) and tau implicated in Alzheimer's disease (Wegmann et al., 2018) become aggregated depending possibly on their concentrations, some time after their formation and/or their chemical modifications. Those proteins are irreversibly aggregated and become dysfunctional, attenuating the neuronal activity of the cells. Collectively considering these observations, we speculate that impairment of the normal regulation of the LLPS of ZO-1 due to changes in intracellular or extracellular conditions could be a possible cause for cancer pathology. Therefore, in addition to embryogenesis, investigating the behavior of ZO-1 in adult tissues, especially in pathological conditions, would deepen the understanding of the physiological significance of the ZO-1 reservoir in cells.

Acknowledgments

R26-ZO-1-GFP mice were provided by LARGE, BDR (accession # CDB026K), RIKEN, Japan. We thank Dr. Fumio Matsuzaki, RIKEN, for human ZO-1 cDNA, Dr. Makoto Suzuki, Hiroshima University, for the GFP-ZO-1/pCS2 construct, and Dr. Lance Davidson, University of Pittsburgh, for the mCherry-Utrophin construct. We thank Dr. Yuko Mimori-Kiyosue, RIKEN, for A6 cells and Dr. Mitsuru Nishita, Fukushima Medical University, and Dr. Kensaku Mizuno, Tohoku University, for MDCK I cells. We thank the BioImaging Facility, Core Research Facilities of the National Institute for Basic Biology (NIBB), for providing us with technical support for live imaging and FRAP analysis. We also thank Dr. Nobuyuki Shiina, NIBB, and Dr. Michael Levine, Princeton University, for technical advice and useful discussion on LLPS and insightful comments on this work. This research was supported by JSPS KAKENHI 20K06663 to NK, JSPS KAKENHI 17H03689 and 16H06280 to TF, and MEXT KAKENHI 22127007 and JSPS KAKENHI 15H05865 to NU. TF and NU were also supported by JST CREST JPMJCR1654, and Joint Research of the Exploratory Research Center on Life and Living Systems (ExCELLS), respectively.

375 **Figure legends**

376

377 **Figure 1. Change of ZO-1 localization in mouse hatching embryos.**

378 **A**. Schematic diagram of the hatching process of the mouse embryo. At E3.5, the
379 embryo is covered with the zona pellucida (ZP). During hatching, the embryo is
380 enlarged with an expansion of trophectoderm (TE) and emerges from the ZP. **B**.
381 Immunofluorescence of mouse E3.5 and E4.5 embryos. Embryos were stained with an
382 anti-ZO-1 antibody, Hoechst 33342 and Alexa Fluor 546 Phalloidin. Scale bar, 20 μm.
383 The inset in the E3.5 phalloidin image was acquired with higher laser power,
384 demonstrating that the structure of cortical F-actin is formed at E3.5 even though the
385 signal intensity was weaker than that in the E4.5 embryo. The bottom panels are
386 enlarged images from the middle panels indicated by white squares. **C - G**. Quantitative
387 analyses of mouse embryos. The nuclear-dense inner cell mass (ICM) region was
388 determined by Hoechst staining. 'Polar' indicates TE to which ICM was attached, and
389 'mural' includes TE to which ICM was not attached. 4 - 5 embryos were analyzed for
390 each condition. **C**. The signal intensities of ZO-1 at the cell periphery of the mural TE at
391 E3.5 and E4.5 were quantified. **D**. The number of particles in one TE cell was counted.
392 **E**. The areas of the TE cells were quantified. **F**. Fluorescence intensity of whole
393 embryos stained with the anti-ZO-1 antibody and phalloidin was measured. For
394 comparison, intensities were normalized by Hoechst staining intensity. n = 5 embryos.
395 **G**. The signal intensities of ZO-1 and phalloidin at the cell periphery of the mural and
396 polar TE of E4.5 embruyos were quantified. n.s.: not significant. *$p < 0.01$.

397

398 **Figure 2. Expansion of TE regulates ZO-1 localization.**

399 **A and B**. Embryos were obtained at E3.5 and cultured for 24 h in the absence (A) or
400 presence of 0.3 mM ouabain (+Ob) (B). Embryos were immunostained with the anti-
401 ZO-1 antibody (left) and the images were analyzed using particle analysis in Image J
402 (right). **C-E**. The percentage of the particle area (C), number of particles (D) and cell
403 size (E) of E4.5 mural TE cells were quantified and plotted. **F**. E4.5 mouse embryos
404 expressing ZO-1-GFP were pierced with a glass needle. Pierced embryos shrank
405 immediately and the recovery process was imaged. **G**. The fluorescence intensity of
406 GFP-ZO-1 at the cell periphery at 0 h and 6 h were quantified. The X-axis indicates
407 distance from the cell membrane. Scale bars, 20 μm. *$p < 0.01$.

408

409 **Figure 3. ZO-1 localization is regulated by F-actin in A6 cells.**

410 **A**. Domain structure of ZO-1 protein and expression constructs used here, GFP-tagged
411 full-length human ZO-1 (GFP-ZO-1), actin-binding domain (ABD)-deletion mutant
412 (GFP-ZO-1ΔABD), GFP-ZO-1ΔC and GFP-ZO-1ΔN. IDRs were predicted by PrDOS
413 (protein disorder prediction system) (Ishida and Kinoshita, 2007). **B**. GFP ZO-1 was
414 transiently expressed in *Xenopus laevis* A6 kidney cells. Cells were fixed and stained
415 with fluorescent phalloidin. **C**. Localization of GFP-ZO-1 and GFP-ZO-1ΔABD. **D**.
416 Localization of GFP-ZO-1 ΔC and ΔN. **E**. GFP-ZO-1 was co-expressed with actin-
417 binding constructs tagged with a red fluorescent protein. Lifeact-RFP, mCherry-
418 Utrophin and RFP-MoesinABD (actin-binding domain). **F**. A6 cells expressing GFP-
419 ZO-1 were treated with 0.5 μM latrunculin B for 20 min, which was then washed out.
420 Scale bars, 20 μm.

421

422 **Figure 4. Dynamics of GFP-ZO-1 particles expressed in A6 and MDCK cells.**

423 **A**. GFP-ZO-1 was transiently expressed in MDCK cells. When MDCK cells were
424 sparsely distributed, GFP-ZO-1 formed cytoplasmic puncta. When GFP-ZO-1 was
425 expressed in densely cultured MDCK cells, ZO-1 localization was different (see Figure
426 6A and the main text). In this figure, sparsely-distributed cells were shown. **B.** The size
427 of ZO-1 puncta in A6 cells co-expressed with MoesinABD and in MDCK cells were
428 compared. **C** and **E**. GFP-ZO-1 in A6 cells co-expressing MoesinABD. **D** and **F**. GFP-
429 ZO-1 in MDCK cells. **C** and **D**. Cells expressing GFP-ZO-1 were semi-permeabilized
430 with 0.012% digitonin. The size of puncta was quantified with Image J particle analysis.
431 n = 12 and 6 puncta, respectively. **E** and **F**. Fluorescent recovery after photobleaching
432 (FRAP) assay. The recovery of fluorescence was quantified. n = 20 puncta. Scale bars,
433 20 μm.

434

435 **Figure 5. Dynamics of ZO-1 puncta in MDCK and A6 cells.**

436 **A** and **B**. GFP-ZO-1 was expressed in MDCK cells, forming islands. In cells located
437 inside of islands (indicated by arrowheads), GFP-ZO-1 was localized mainly at the
438 plasma membrane. In contrast, in cells at the periphery or outside of the colony
439 (indicated by arrows), GFP-ZO-1 formed puncta. **C**. MDCK cells that formed a colony
440 were immunostained with the anti-ZO-1 antibody. Images were analyzed using 'particle

441 analysis' in Image J software. **D**. Cells in the island were divided into three groups with
442 respect to their location, namely the first and second rows from the edge, and the central
443 region of the island. The number of particles in each cell was counted. n = 20 cells. *p <
444 0.01. **E-G.** Laser ablation of MDCK cells expressing GFP-ZO-1. **E**. Cells inside of an
445 island which had GFP-ZO-1 around the cell membrane. About 80% of these cells
446 remained stable after ablation (Video S7). **F**. A cell located close to the edge of an
447 island, and which had GFP-ZO-1 puncta. About 80% of these cells rapidly erupted and
448 detached from the bottom of the dish (Video S8). Arrowheads indicate laser ablation
449 sites. **G**. A statistical summary of the laser ablation experiment. "attached" indicates
450 cells that stayed attached to the dish after ablation, as shown in **E**. "erupted" indicates
451 cells that erupted after ablation and detached from the dish, as shown in **F**. Data were
452 obtained from two experiments. The total numbers of cells for the laser ablation were 26
453 inside and 24 outside cells. Scale bars, 20 μm.
454
455 **Figure 6. Wound-healing assay using MDCK cells expressing GFP-ZO-1**
456 **A** and **B**. The confluent cell sheet was scratched and observed. Just after scratching (0
457 h), GFP-ZO-1 was at the cell periphery, whereas after 3 hours (3 h), it formed puncta in
458 many of the cells close to the scratch (within 200 μm). Cells in **B** were magnified from
459 #1 and #2 cells in **A**. Scale bar, 20 μm. **C**. The number of cells with GFP-ZO-1 particles
460 were counted. Cells located within 200 μm from the scratch site were defined as "edge"
461 cells. Cells more than 200 μm away from the scratch site were defined as "inner" cells.
462 The data were obtained from three experiments. **D** and **E**. Inner and edge cells were
463 fixed 10 h after scratching and stained with phalloidin. The arrow indicates the wound
464 site. Scale bar, 20 μm. **F**. Fluorescence intensity of phalloidin staining at the plasma
465 membrane was measured. *p < 0.01.
466

467 **Supplementary Figure and Video Legends**

468 **Figure S1. E3.5 and E4.5 embryos expressing ZO-1-EGFP (related to Figure 1)**

469 **A**. Embryos from mice expressing ZO-1-EGFP by EGFP-knock-in were observed.
470 Before hatching (E3.5), ZO-1 puncta were observed around the cell periphery, but cell-
471 cell boundaries were not clear. After hatching (E4.5), membrane localization of ZO-1-
472 GFP became evident. The signal around the nuclei in the TE and large puncta in the
473 ICM are autofluorescence, which was confirmed by observation of wild-type mouse
474 embryos not expressing ZO-1-GFP (data not shown). **B**. Mouse E3.5 and E4.5 embryos
475 expressing ZO-1-EGFP at higher magnification. **C**. Fluorescence intensity around cell
476 boundaries in ZO-1-EGFP–expressing embryos was quantified. After hatching, ZO-1-
477 EGFP localized to the plasma membrane and formed sharp boundaries with ZO-1-
478 EGFP. Scale bars, 20 μm.

479

480 **Figure S2. Immunofluorescence of mouse E4.5 embryos pierced with a glass needle**
481 **(related to Figure 2)**

482 **A**. Mouse E4.5 embryos expressing ZO-1-GFP were pierced with a glass needle, then
483 the volume of the blastocyst cavity was reduced, and embryos shrank. Those embryos
484 were fixed and immunostained. **B**. The number of particles was counted using Image J
485 particle analysis. **C**. The area of particles and cytoplasm of one mural TE cell was
486 measured by Image J software, and the ratio of those values was plotted. *$p < 0.01$.

487

488 **Figure S3. Dynamics of GFP-ZO-1 puncta in A6 cell co-expressing RFP-**
489 **MoesinABD (related to Figure 3)**

490 Puncta often underwent fission and fusion, as indicated by arrowheads. These images
491 are from Video S3.

492

493 **Figure S4. Trypsin-EDTA treatment of confluently growing MDCK cells**
494 **expressing GFP-ZO-1 (related to Figure 5)**

495 As cells lost their cell-cell contact and their shape became spherical, ZO-1 detached
496 from the plasma membrane and formed puncta. These images are from Video S9.

497

498 **Figure S5. Localization of GFP-ZO-1 in a wound-healing assay and in osmolarity**
499 **change in MDCK cells (related to Figure 6)**

500 **A-C. Wound-healing assay followed by FRAP assay. A**. Cells that formed GFP-ZO-1
501 puncta in the wound-healing assay. The cell indicated by the square and the arrowhead
502 was used for the following FRAP assay. **B** and **C**. GFP-ZO-1 puncta formed during
503 wound healing were subjected for the FRAP assay. Three cells were analyzed. **D**. An A6
504 cell expressing GFP-ZO-1 was treated with a high-salt medium (four-fold higher
505 concentration of PBS) for 40 min then returned to standard medium. Scale bars, 20 μm.
506
507 **Video S1.** Mouse embryos expressing ZO-1-EGFP were flushed from uteri at one-day
508 post-coitum and observed by time-lapse microscopy for 92 h (related to Figure S1).
509
510 **Video S2**. Mouse E4.5 embryos expressing ZO-1-EGFP were pierced by a glass needle
511 and observed by time-lapse microscopy (related to Figure 2F).
512
513 **Video S3.** An A6 cell co-expressing GFP-ZO-1 and RFP-MoesinABD was imaged by
514 time-lapse microscopy for 885 min (related to Figure S3).
515
516 **Video S4.** Latrunculin B treatment of an A6 cell co-expressing GFP-ZO-1 and RFP-
517 MoesinABD (related to Figure 3F).
518
519 **Video S5.** A6 cells co-expressing GFP-ZO-1 and RFP-MoesinABD were treated with
520 digitonin ("+digitonin" at 50 sec in the video) and imaged by time-lapse microscopy
521 (related to Figure 4C).
522
523 **Video S6.** An MDCK cell expressing GFP-ZO-1 was treated with digitonin
524 ("+digitonin" at 50 sec in the video) and imaged by time-lapse microscopy (related to
525 Figure 4D).
526
527 **Video S7.** Laser ablation of MDCK cells expressing GFP-ZO-1 inside of the island. The
528 laser was irradiated at 4 sec at the membrane indicated by arrowheads (related to Figure
529 5E).
530
531 **Video S8.** Laser ablation of MDCK cells expressing GFP-ZO-1 at the periphery of the
532 island. The laser was irradiated at 4 sec at the membrane indicated by the arrowhead.

533 The cell erupted and disappeared immediately after irradiation (related to Figure 5F).
534
535 **Video S9.** MDCK cells expressing GFP-ZO-1 were treated with a trypsin-EDTA
536 solution. The video starts immediately after treatment (related to Figure S4).
537
538 **Video S10.** A wound-healing assay of MDCK cells. A sheet of MDCK cells transfected
539 with the GFP-ZO-1 construct was scratched and observed by time-lapse microscopy
540 (related to Figure 6).
541
542 **Video S11.** A wound-healing assay of MDCK cells, followed by a FRAP assay (1). A
543 sheet of MDCK cells transfected with the GFP-ZO-1 construct was scratched and
544 observed by time-lapse microscopy (related to Figure S5A). The cell for the following
545 FRAP assay was indicated by an arrowhead at the first and the last frames.
546
547 **Video S12.** A wound-healing assay of MDCK cells, followed by a FRAP assay (2).
548 FRAP assay was conducted using a cell in Video S11 which formed ZO-1 puncta
549 (related to Figure S5B). The granule bleached in the FRAP assay was indicated by an
550 arrowhead.
551
552 **Video S13.** A6 cell expressing GFP-ZO-1 was treated with a high-salt medium (four-
553 fold higher concentration of PBS) at the 4-min time point indicated by "+osmo" in the
554 video and then returned to normal medium at the 55-min time point indicated by "wash
555 out" (related to Figure S5D)..
556

557 **Methods**

558 **KEY RESOURCES TABLE**

REAGENT or RESOURCE	SOURCE	IDENTIFIER
Antibodies		
anti-ZO-1 antibody	Thermo Fisher Scientific	cat. # 33-9100; RRID:AB_2533147
goat anti-mouse IgG antibody, Alexa Fluor 488	Thermo Fisher Scientific	cat. # A28175; RRID:AB_2536161
Chemicals, Peptides, and Recombinant Proteins		
Blocking One	Nacalai Tesque	cat.# 03953
KSOM	Millipore	cat. # MR-106D
ouabain	Sigma	cat.# O3125
Alexa Fluor 546 Phalloidin	Thermo Fisher Scientific	cat.# A22283; RRID:AB_2632953
Hoechst 33342	Thermo Fisher Scientific	cat.# H3570
Lipofectamine 2000	Invitrogen	cat. # 11668-027
Effectene	Qiagen	cat. # 301425
Latrunculin B	Enzo Life Science	cat. # BML-T110-0001
digitonin	WAKO	cat. # 048-02124
trypsin	Nacalai Tesque	cat # 35555-54
Experimental Models: Organisms/Strains		
Xenopus laevis (J-strain)	N/A	N/A
R26-ZO-1EGFP	RIKEN	accession # CDB026K
wild type ICR mice	Japan CREA	N/A
Experimental Models: Cell Lines		

MDCK I cells	Fujiwara et al. (2016)	N/A
A6 cells	Mimori-Kiyosue et al. (2007)	N/A
Recombinant DNA		
human ZO-1	Konno et al. (2008)	N/A
GFP-ZO-1/pCS2	This paper	N/A
GFP-ZO-1 Δ ABD/pCS2 (Δ1151-1371)	This paper	N/A
GFP-ZO-1ΔC/pCS2 (Δ595-1748)	This paper	N/A
GFP-ZO-1ΔN/pCS2 (Δ1-594)	This paper	N/A
Lifeact-RFP	Iioka et al. (2007)	N/A
RFP-MoesinABD	Iioka et al. (2004)	N/A
mCherry-Utrophin	Kim and Davidson (2013)	N/A
Software and Algorithms		
Fiji	NIH	https://fiji.sc
Python 3.6	Python Core Team	https://www.python.org
Pandas	v0.22	http://pandas.pydata.org
seaborn	v0.8	https://seaborn.pydata.org
Matplotlib	v2.2	https://matplotlib.org
Andor IQ2	Oxford Instruments	https://andor.oxinst.com/products/iq-live-cell-imaging-software/
PrDOS (protein disorder prediction system)	(Ishida and Kinoshita, 2007)	http://prdos.hgc.jp/cgi-bin/top.cgi

559

Lead Contact and Materials Availability

Further information and requests for resources and reagents should be directed to and will be fulfilled by the Lead Contact, Naoto Ueno (nueno@nibb.ac.jp.). All unique/stable reagents generated in this study are available from the Lead Contact with a completed Material Transfer Agreement.

Method details

Mouse embryo collection

Animal care and experiments were conducted in accordance with the Guidelines of Animal Experimentation of the National Institutes for Natural Sciences. All animal experiments were approved by the Animal Research Committee of the National Institutes for Natural Sciences. Mice were maintained in a light- and temperature-controlled room using a 12 h light:12 h dark cycle at 23+/-2 °C.

Males of R26-ZO-1EGFP (Katsunuma et al., 2016) or wild type ICR (Japan CREA) were mated with wild type ICR females to obtain blastocysts. Preimplantation E3.5 embryos were flushed from uteri with KSOM (MR-106D, Millipore). Embryos were cultured in KSOM covered with mineral oil at 37 °C and 5% CO_2. Fluorescent signals were monitored using a confocal microscope (A1, Nikon) or a spinning disc confocal microscope (CV1000 ,Yokogawa). For immunofluorescence, embryos were fixed at 4 °C in 4% paraformaldehyde (PFA) in PBS overnight. For ouabain treatment, 10 mM ouabain (cat. # O3125, Sigma) in DMSO were diluted to the indicated concentrations.

Manipulation of mouse embryos

To remove the zona pellucida, embryos were treated with Tyrode's solution (Bradley, 1987). Embryos were transferred to a drop of Tyrode's solution. The zona was removed typically within 1 min. Then, embryos were washed three times in KSOM. To pierce the mural trophectoderm, microinjection needles were made from a 1 mm diameter glass capillary (GD1, Narishige), the needle was set to a micromanipulator (Leica), and embryos were pierced with the needle by manual manipulation.

593 **Immunofluorescence with mouse embryos**
594 Fixed embryos were washed three times with 1% bovine serum albumin (BSA) in PBS,
595 and then soaked in a blocking solution, 0.1% Triton X-100 in Blocking One (cat. #
596 03953, Nacalai, Japan) for 1 h at room temperature. Then, the embryos were incubated
597 in the primary antibody solution containing an anti-ZO-1 antibody (cat. # 33-9100,
598 Thermo) diluted 100-times in Blocking One at 4 °C overnight. After washing three
599 times with the blocking solution, embryos were incubated in a secondary antibody
600 solution containing 100-times diluted goat anti-mouse IgG antibody Alexa Flour 488
601 (cat. # A27185, Thermo), 100-times diluted Alexa Fluor 546 Phalloidin (cat. # A22283,
602 Thermo Fisher), and 10 μg/ml Hoechst 33342 (cat. # H3570, Thermo Fisher) in
603 Blocking One. Fluorescent signals were monitored using Nikon A1 or Leica SP8
604 confocal microscopes.
605
606 **Measurement of fluorescent intensities and particle analyses**
607 Fiji/Image J was used to measure fluorescent intensities. Particle analyses in Fiji/Image
608 J were used to count the numbers of particles and measure particle areas. Images were
609 converted to an 8-bit type, and cytoplasmic regions were manually determined. The
610 "analysis particles" program was run with the threshold signal value set at 20, and
611 circularity was 0.25-1.0 for the definition of particles.
612
613 **GFP-ZO-1 expression constructs**
614 Human ZO-1 cDNA was a gift from Dr. Fumio Matsuzaki (Konno et al., 2008)). EGFP-
615 human ZO-1/pCS2 was constructed by Dr. Makoto Suzuki. ZO-1ΔABD lacks amino
616 acid (aa) # 1151-1371. ZO-1ΔC lacks aa # 595-1748. ZO-1-1ΔN lacks aa # 1-594.
617 Lifeact-RFP is described in Iioka et al. (2007). MoesinABD is described in Iioka et al.
618 (2004). The mCherry-Utrophin construct was a gift from Lance A. Davidson (Kim and
619 Davidson, 2013).
620
621 **Cell culture and transfection of plasmids**
622 A6 cells, established from a normal *X. laevis* kidney, were a gift from Dr. Yuko Mimori-
623 Kiyosue (Mimori-Kiyosue et al., 2007). A6 cells were grown at 24 °C without CO_2 in
624 Leibovitz's L-15 medium (50% L-15 medium, 10% fetal bovine serum (FBS), 200 mg/l
625 kanamycin). MDCK cells were a gift from Dr. Mitsuru Nishita and Dr. Kensaku

626 Mizuno. MDCK cells were cultured in Dulbecco's modified Eagle medium (DMEM)
627 containing 10% FBS. Transfection was conducted using Lipofectamine 2000
628 (Invitrogen # 11668-027) for MDCK cells and Effectene (Qiagen # 301425) for A6 cells
629 following the manufacturers' instructions.
630
631 **Immunofluorescence of the tissue culture cells**
632 Cells were fixed in 4% PFA in PBS at 4 °C overnight, washed with 0.1% Triton X-100
633 in PBS. Blocking One (cat. # 03953, Nacalai Tesque, Japan) was used to block for 1 h at
634 room temperature, followed by incubation in the primary antibody solution, a 100-times
635 diluted anti-ZO-1 antibody (cat. # 33-9100, Thermo) in Blocking One at 4 °C overnight.
636 After washing three times in Blocking One, cells were incubated in the secondary
637 antibody solution containing 200-times diluted goat anti-mouse IgG antibody Alexa
638 Flour 488 (cat. # A27185, Thermo) and 200-times diluted Alexa Fluor 546 Phalloidin
639 (cat. # A22283, Thermo Fisher) in Blocking One at 4 °C overnight. After washing three
640 times in PBS, cells were observed using a Leica SP8 confocal microscope.
641
642 **Laser ablation**
643 Laser ablation was conducted using an Olympus IX 81 inverted microscope (20 x /0.70
644 NA dry objective lens), equipped with a spinning-disc confocal unit Yokogawa CSUX-1
645 and iXon3 897 EM-CCD camera (Andor), controlled with Andor IQ2 software. An N2
646 Micropoint laser (16 Hz, 365 nm, 2.0 μW, Photonic Instruments) was focused on the
647 membrane at the cell membrane. Time-lapse images were acquired every 200 msec
648 before and during the laser ablation process and analyzed with Fiji software.
649
650 **Fluorescence recovery after photobleaching (FRAP)**
651 FRAP assays in the tissue culture cells were conducted with a Leica SP8 confocal
652 microscope and software equipped in the microscope operating system. Regions of
653 interest (ROI) were bleached using a 488 nm laser. Pre-bleach and post-bleach images
654 were acquired with a 488 nm laser. Fluorescence recovery of GFP-ZO-1 was monitored.
655 Recovery data were background corrected and normalized to the ROI intensity before
656 bleaching. A reference ROI outside the bleached area was processed in the same way.
657
658 **Observation of GFP-ZO-1 dynamics in the tissue culture cells**

659 For the wound-healing assay, MDCK cells almost confluently grown on a glass-bottom
660 dish were transfected with GFP-ZO-1/pCS2. After one day, the cell layer was scratched
661 with a Pipetman tip, incubated at 37 °C, 5% CO_2 in a stage-top incubator (cat. # STXG,
662 Tokai HIT, Japan) and observed by a Leica SP8 confocal microscope.
663 For the latrunculin B treatment, 2.5 μM latrunculin B in the culture medium was added
664 to the culture dish of A6 cells transiently expressing GFP-ZO-1 so that the final
665 concentration of latrunculin B was 0.5 μM. For digitonin treatment, 0.06% digitonin in
666 the culture medium was added to the culture dish so that the final concentration of
667 digitonin was 0.012%. For hyperosmolarity treatment of A6 cells, 10 x PBS was added
668 so that the concentration of PBS changed from 0.5 x to 1.5 x. Cells were observed at
669 room temperature. For the trypsin-EDTA treatment, the culture medium of MDCK cells
670 was replaced with PBS containing 0.05% trypsin and 1 mM EDTA.
671

672 **References**

673

674 Anderson, J.M., Stevenson, B.R., Jesaitis, L.A., Goodenough, D.A., and Mooseker, M.S.
675 (1988). Characterization of ZO-1, a protein component of the tight junction from mouse
676 liver and Madin-Darby canine kidney cells. J Cell Biol *106*, 1141-1149.
677 Baum, B., Settleman, J., and Quinlan, M.P. (2008). Transitions between epithelial and
678 mesenchymal states in development and disease. Semin Cell Dev Biol *19*, 294-308.
679 Beutel, O., Maraspini, R., Pombo-Garcia, K., Martin-Lemaitre, C., and Honigmann, A.
680 (2019). Phase Separation of Zonula Occludens Proteins Drives Formation of Tight
681 Junctions. Cell *179*, 923-936.
682 Bodor, D.L., Ponisch, W., Endres, R.G., and Paluch, E.K. (2020). Of Cell Shapes and
683 Motion: The Physical Basis of Animal Cell Migration. Dev Cell *52*, 550-562.
684 Bradley, A. (1987). Production and analysis of chimeric mice. In Teratocarcinoma and
685 Embryonic Stem Cells, E.J. Robertson, ed. (Oxford: IRL Press), pp. 113-151.
686 Brangwynne, C.P. (2013). Phase transitions and size scaling of membrane-less organelles.
687 J Cell Biol *203*, 875-881.
688 Chan, C.J., Costanzo, M., Ruiz-Herrero, T., Monke, G., Petrie, R.J., Bergert, M., Diz-
689 Munoz, A., Mahadevan, L., and Hiiragi, T. (2019). Hydraulic control of mammalian
690 embryo size and cell fate. Nature *571*, 112-116.
691 Choi, Y.S., Sehgal, R., McCrea, P., and Gumbiner, B. (1990). A cadherin-like protein in
692 eggs and cleaving embryos of Xenopus laevis is expressed in oocytes in response to
693 progesterone. J Cell Biol *110*, 1575-1582.
694 Fanning, A.S., Ma, T.Y., and Anderson, J.M. (2002). Isolation and functional
695 characterization of the actin binding region in the tight junction protein ZO-1. FASEB J
696 *16*, 1835-1837.
697 Fujishiro, S.H., Tanimura, S., Mure, S., Kashimoto, Y., Watanabe, K., and Kohno, M.
698 (2008). ERK1/2 phosphorylate GEF-H1 to enhance its guanine nucleotide exchange
699 activity toward RhoA. Biochemical and biophysical research communications *368*, 162-
700 167.
701 Fujiwara, S., Ohashi, K., Mashiko, T., Kondo, H., and Mizuno, K. (2016). Interplay
702 between Solo and keratin filaments is crucial for mechanical force-induced stress fiber
703 reinforcement. Mol Biol Cell *27*, 954-966.
704 Ginsberg, D., DeSimone, D., and Geiger, B. (1991). Expression of a novel cadherin (EP-

705 cadherin) in unfertilized eggs and early Xenopus embryos. Development *111*, 315-325.
706 Godard, B.G., and Heisenberg, C.P. (2019). Cell division and tissue mechanics. Curr Opin
707 Cell Biol *60*, 114-120.
708 Gonzalez-Mariscal, L., Quiros, M., and Diaz-Coranguez, M. (2011). ZO proteins and
709 redox-dependent processes. Antioxid Redox Signal *15*, 1235-1253.
710 Hallou, A., and Brunet, T. (2020). On growth and force: mechanical forces in
711 development. Development *147*, dev187302.
712 Hannezo, E., and Heisenberg, C.P. (2019). Mechanochemical Feedback Loops in
713 Development and Disease. Cell *178*, 12-25.
714 Hashimoto, Y., Kinoshita, N., Greco, T.M., Federspiel, J.D., Jean Beltran, P.M., Ueno, N.,
715 and Cristea, I.M. (2019). Mechanical force induces phosphorylation-mediated signaling
716 that underlies tissue response and robustness in Xenopus embryos. Cell systems *8*, 226-
717 241.
718 Hernandez-Vega, A., Marsal, M., Pouille, P.A., Tosi, S., Colombelli, J., Luque, T.,
719 Navajas, D., Pagonabarraga, I., and Martin-Blanco, E. (2017). Polarized cortical tension
720 drives zebrafish epiboly movements. The EMBO journal *36*, 25-41.
721 Hino, N., Rossetti, L., Marin-Llaurado, A., Aoki, K., Trepat, X., Matsuda, M., and
722 Hirashima, T. (2020). ERK-Mediated Mechanochemical Waves Direct Collective Cell
723 Polarization. Dev Cell *53*, 646-660.
724 Iioka, H., Iemura, S., Natsume, T., and Kinoshita, N. (2007). Wnt signalling regulates
725 paxillin ubiquitination essential for mesodermal cell motility. Nat Cell Biol *9*, 813-821.
726 Iioka, H., Ueno, N., and Kinoshita, N. (2004). Essential role of MARCKS in cortical actin
727 dynamics during gastrulation movements. J Cell Biol *164*, 169-174.
728 Ishida, T., and Kinoshita, K. (2007). PrDOS: prediction of disordered protein regions
729 from amino acid sequence. Nucleic Acids Res *35*, W460-464.
730 Ito, S., Okuda, S., Abe, M., Fujimoto, M., Onuki, T., Nishimura, T., and Takeichi, M.
731 (2017). Induced cortical tension restores functional junctions in adhesion-defective
732 carcinoma cells. Nat Commun *8*, 1834.
733 Itoh, K., Ossipova, O., and Sokol, S.Y. (2014). GEF-H1 functions in apical constriction
734 and cell intercalations and is essential for vertebrate neural tube closure. J Cell Sci *127*,
735 2542-2553.
736 Kato, M., Han, T.W., Xie, S., Shi, K., Du, X., Wu, L.C., Mirzaei, H., Goldsmith, E.J.,
737 Longgood, J., Pei, J.*, et al.* (2012). Cell-free formation of RNA granules: low complexity

738 sequence domains form dynamic fibers within hydrogels. Cell *149*, 753-767.
739 Katsunuma, S., Honda, H., Shinoda, T., Ishimoto, Y., Miyata, T., Kiyonari, H., Abe, T.,
740 Nibu, K., Takai, Y., and Togashi, H. (2016). Synergistic action of nectins and cadherins
741 generates the mosaic cellular pattern of the olfactory epithelium. J Cell Biol *212*, 561-
742 575.
743 Kim, H.Y., and Davidson, L.A. (2013). Investigating morphogenesis in Xenopus
744 embryos: imaging strategies, processing, and analysis. Cold Spring Harb Protoc *2013*,
745 298-304.
746 Kinoshita, N., Hashimoto, Y., Yasue, N., Suzuki, M., Cristea, I.M., and Ueno, N. (2020).
747 Mechanical Stress Regulates Epithelial Tissue Integrity and Stiffness through the
748 FGFR/Erk2 Signaling Pathway during Embryogenesis. Cell Rep *30*, 3875-3888.
749 Konno, D., Shioi, G., Shitamukai, A., Mori, A., Kiyonari, H., Miyata, T., and Matsuzaki,
750 F. (2008). Neuroepithelial progenitors undergo LGN-dependent planar divisions to
751 maintain self-renewability during mammalian neurogenesis. Nat Cell Biol *10*, 93-101.
752 Leonavicius, K., Royer, C., Preece, C., Davies, B., Biggins, J.S., and Srinivas, S. (2018).
753 Mechanics of mouse blastocyst hatching revealed by a hydrogel-based microdeformation
754 assay. Proc Natl Acad Sci U S A *115*, 10375-10380.
755 Li, P., Banjade, S., Cheng, H.C., Kim, S., Chen, B., Guo, L., Llaguno, M., Hollingsworth,
756 J.V., King, D.S., Banani, S.F., *et al.* (2012). Phase transitions in the assembly of
757 multivalent signalling proteins. Nature *483*, 336-340.
758 Mimori-Kiyosue, Y., Matsui, C., Sasaki, H., and Tsukita, S. (2007). Adenomatous
759 polyposis coli (APC) protein regulates epithelial cell migration and morphogenesis via
760 PDZ domain-based interactions with plasma membranes. Genes Cells *12*, 219-233.
761 Murray, D.T., Kato, M., Lin, Y., Thurber, K.R., Hung, I., McKnight, S.L., and Tycko, R.
762 (2017). Structure of FUS Protein Fibrils and Its Relevance to Self-Assembly and Phase
763 Separation of Low-Complexity Domains. Cell *171*, 615-627.
764 Paolini, A., and Abdelilah-Seyfried, S. (2018). The mechanobiology of zebrafish cardiac
765 valve leaflet formation. Curr Opin Cell Biol *55*, 52-58.
766 Ren, Y., Li, R., Zheng, Y., and Busch, H. (1998). Cloning and characterization of GEF-
767 H1, a microtubule-associated guanine nucleotide exchange factor for Rac and Rho
768 GTPases. J Biol Chem *273*, 34954-34960.
769 Schwayer, C., Shamipour, S., Pranjic-Ferscha, K., Schauer, A., Balda, M., Tada, M.,
770 Matter, K., and Heisenberg, C.P. (2019). Mechanosensation of Tight Junctions Depends

771 on ZO-1 Phase Separation and Flow. Cell *179*, 937-952.
772 Shiina, N. (2019). Liquid- and solid-like RNA granules form through specific scaffold
773 proteins and combine into biphasic granules. J Biol Chem *294*, 3532-3548.
774 Teng, X., Qin, L., Le Borgne, R., and Toyama, Y. (2017). Remodeling of adhesion and
775 modulation of mechanical tensile forces during apoptosis in Drosophila epithelium.
776 Development *144*, 95-105.
777 Thompson, D.W. (1917). On Growth and Form (Cambridge Univ. Press).
778 Wegmann, S., Eftekharzadeh, B., Tepper, K., Zoltowska, K.M., Bennett, R.E., Dujardin,
779 S., Laskowski, P.R., MacKenzie, D., Kamath, T., Commins, C.*, et al.* (2018). Tau protein
780 liquid-liquid phase separation can initiate tau aggregation. The EMBO journal *37*, e98049.
781

Kinoshita et al. Figure 1

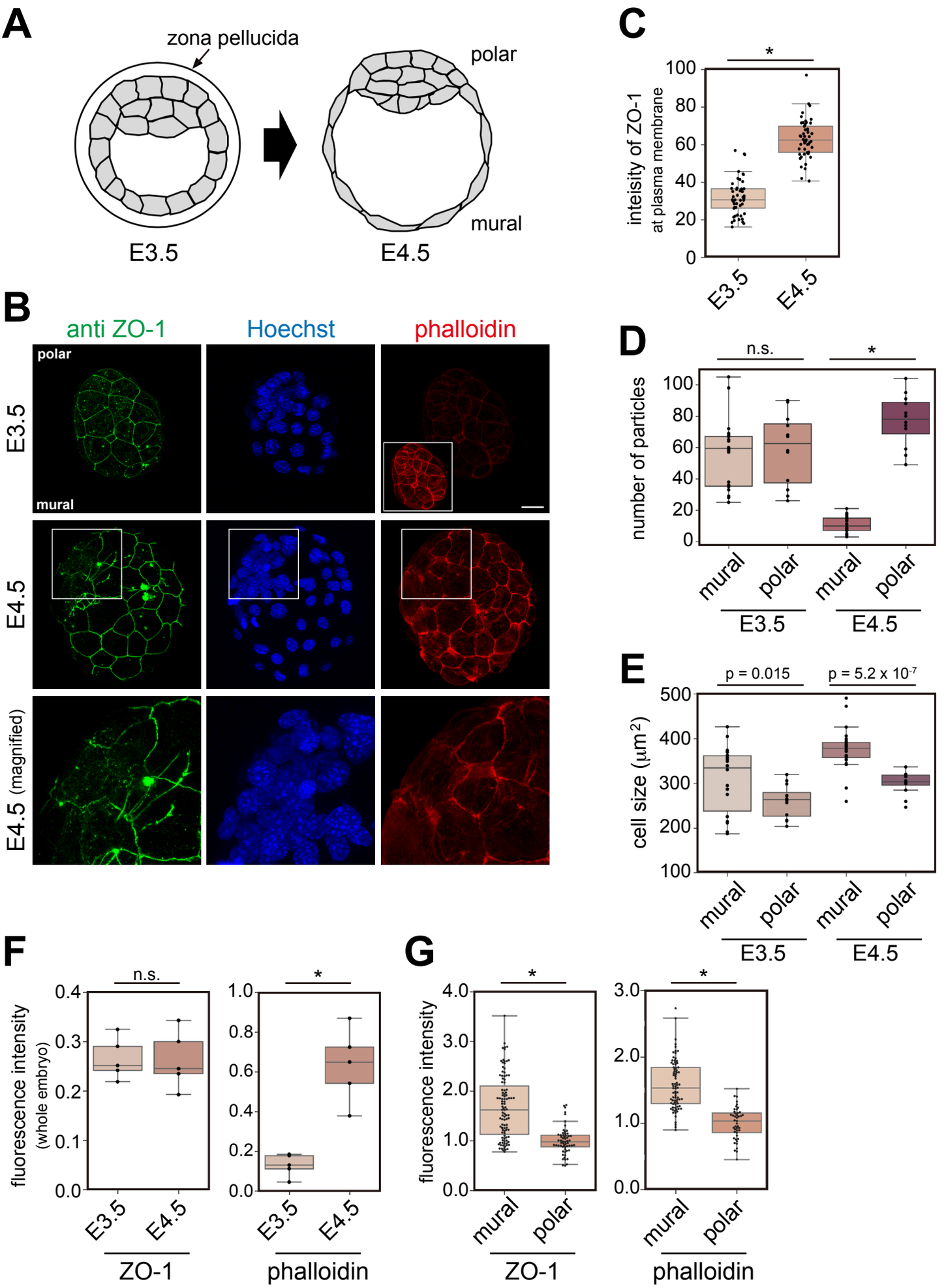

Kinoshita et al. Figure 2

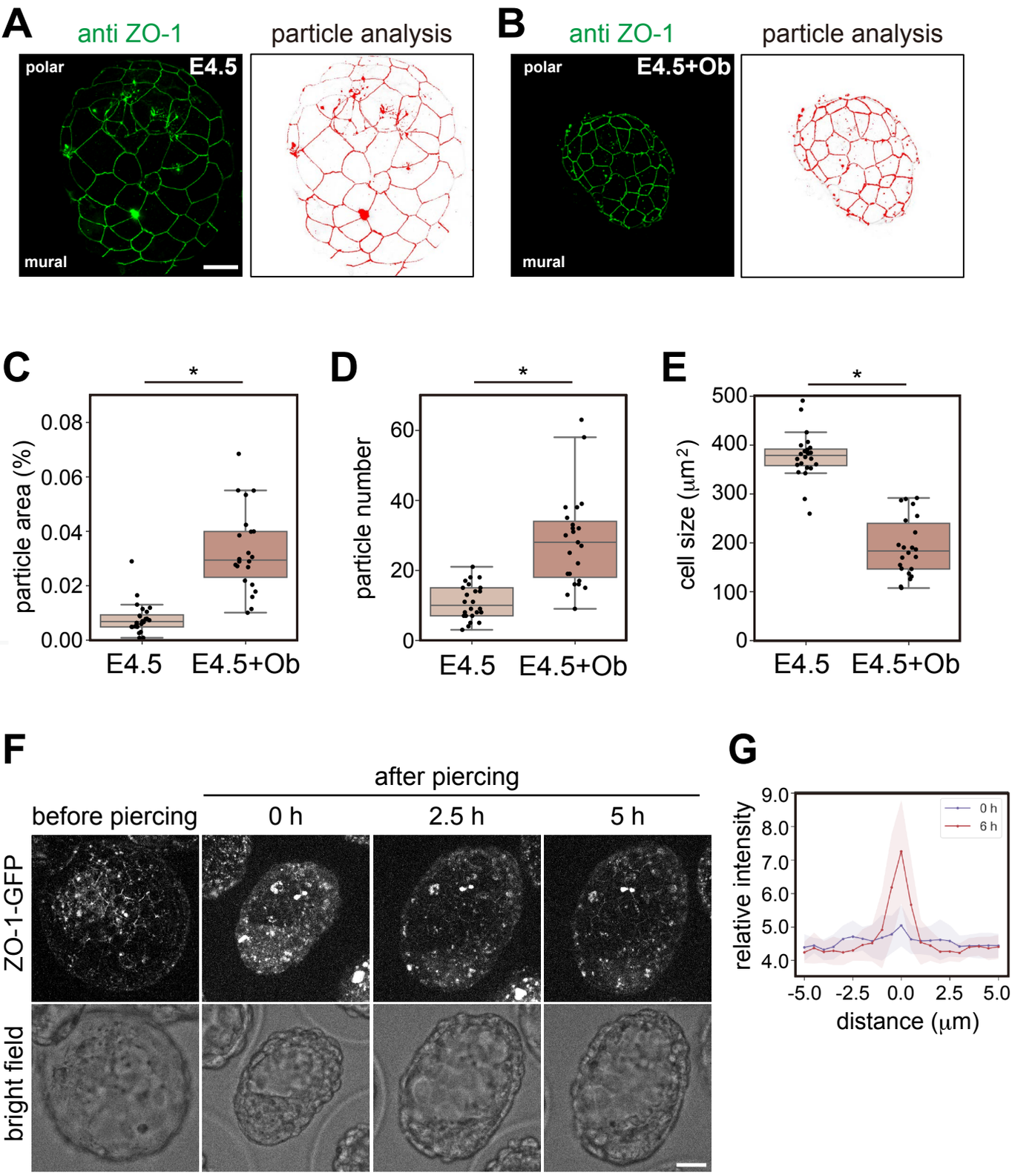

Kinoshita et al. Figure 3

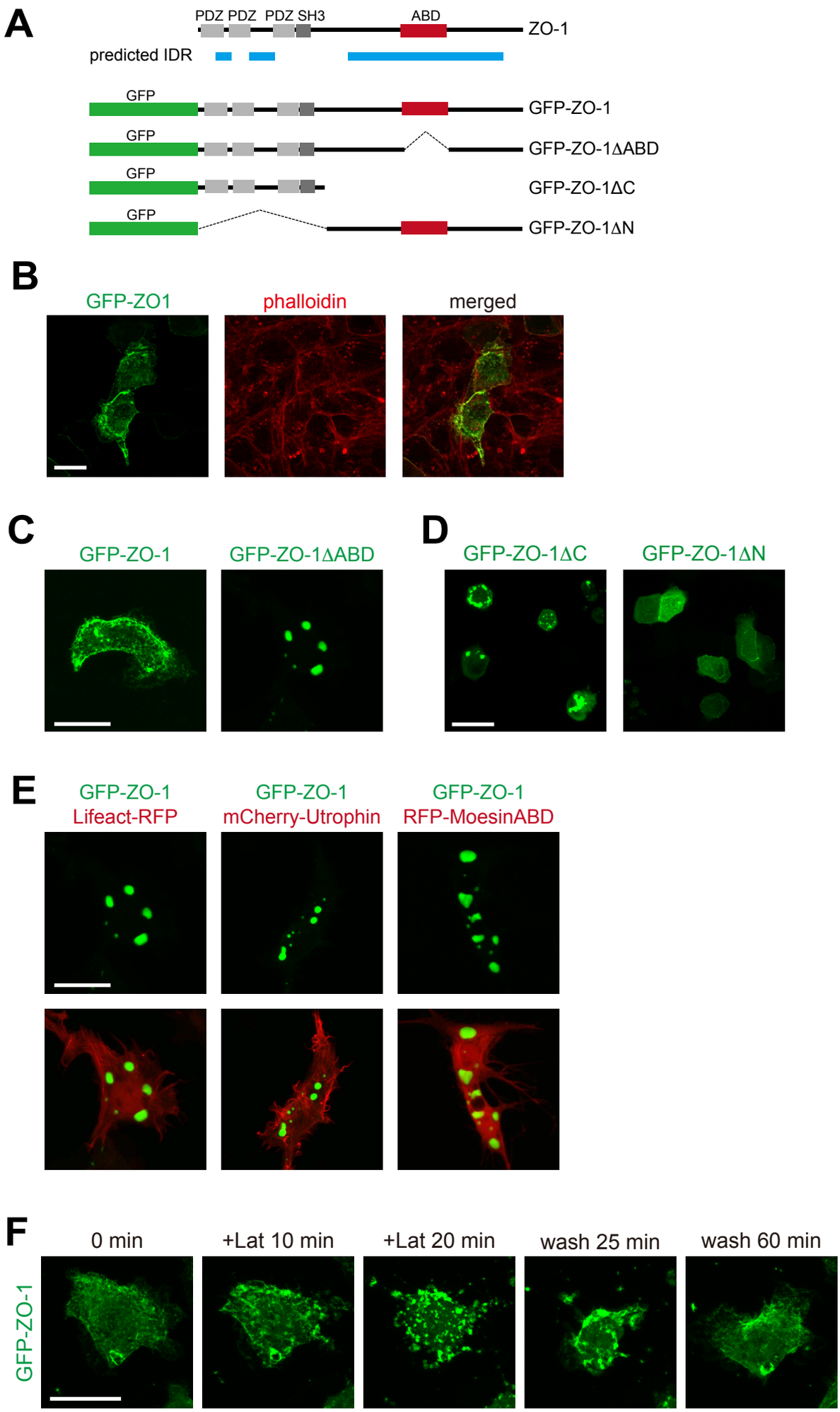

Kinoshita et al. Figure 4

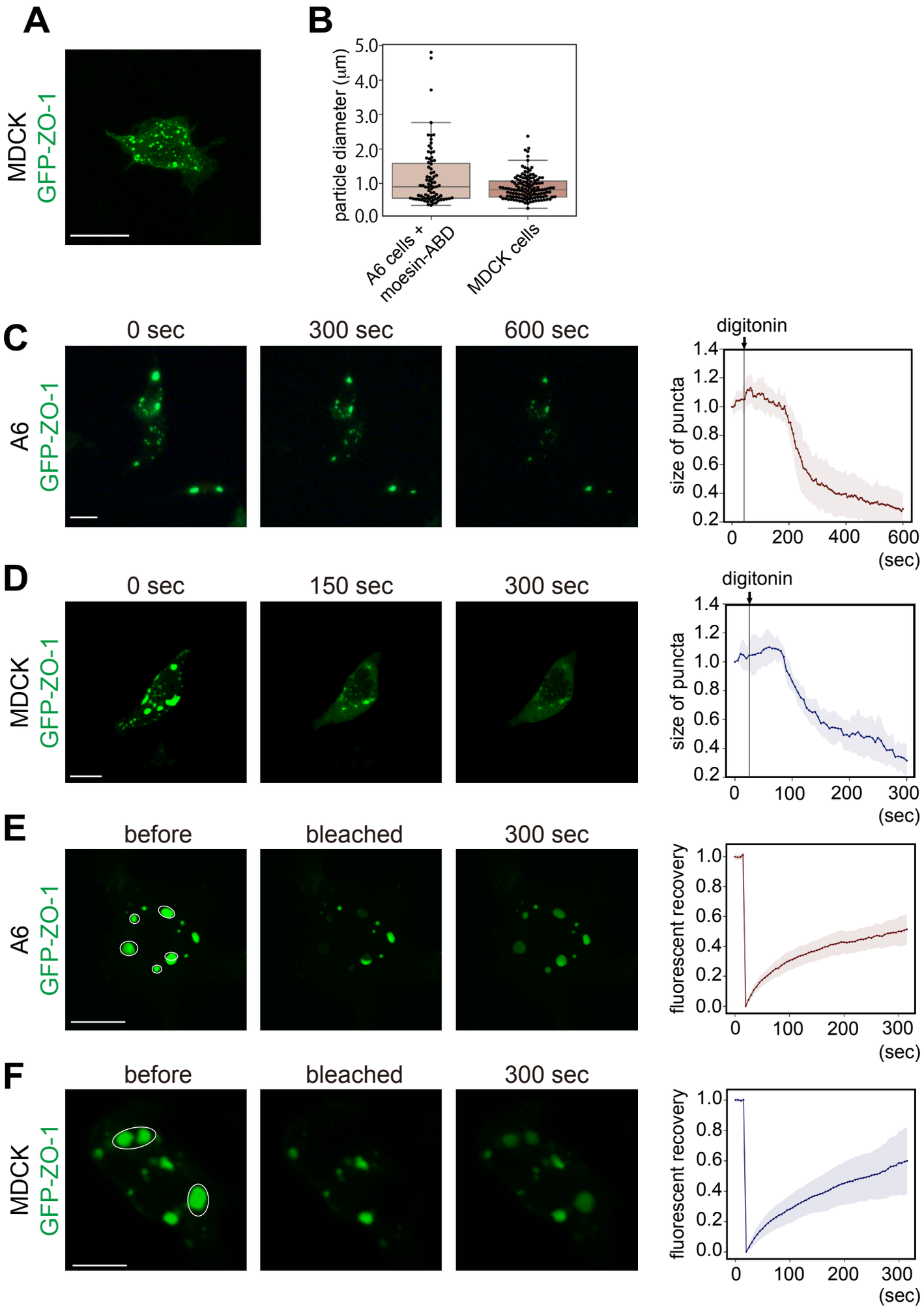

Kinoshita et al. Figure 5

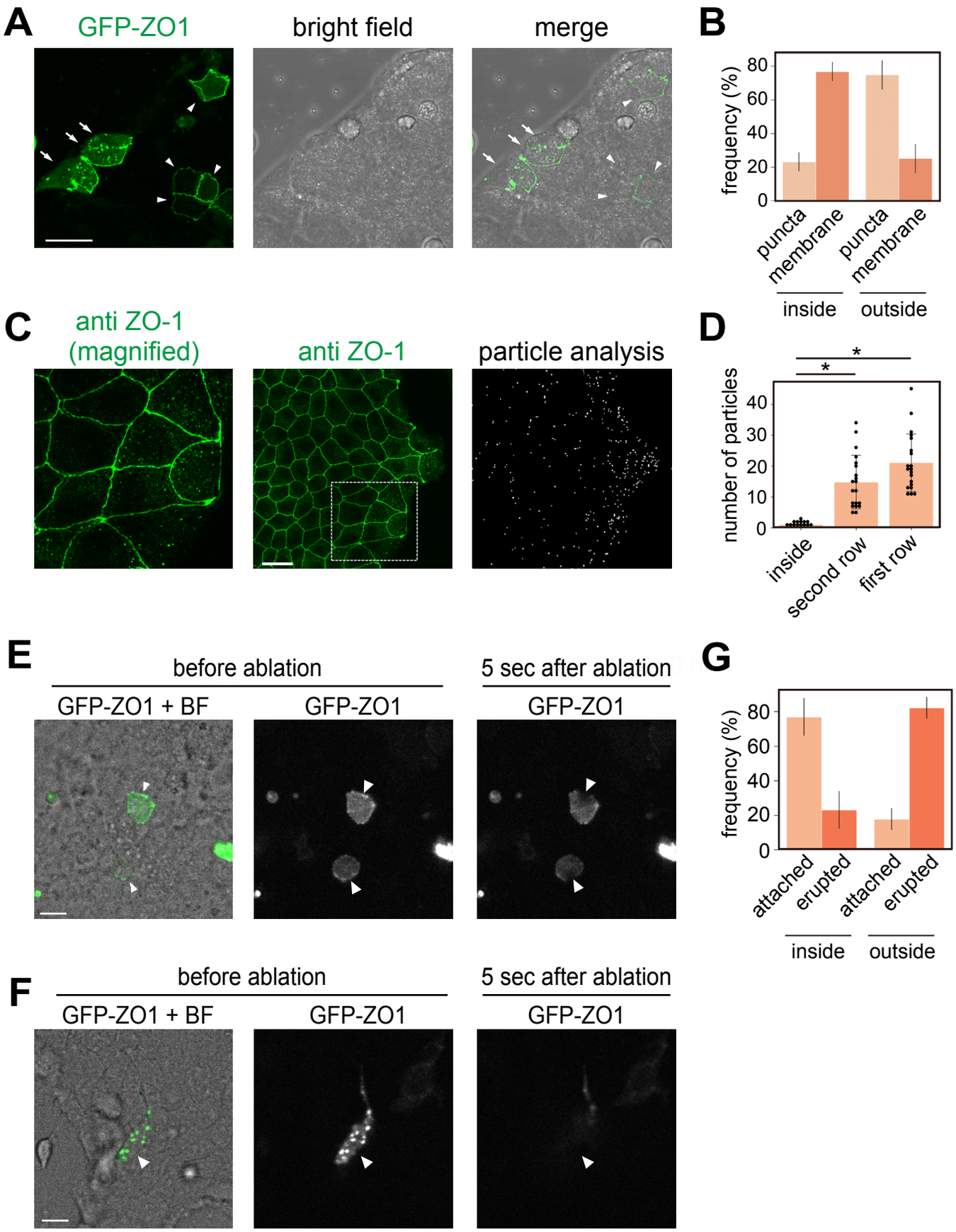

Kinoshita et al. Figure 6

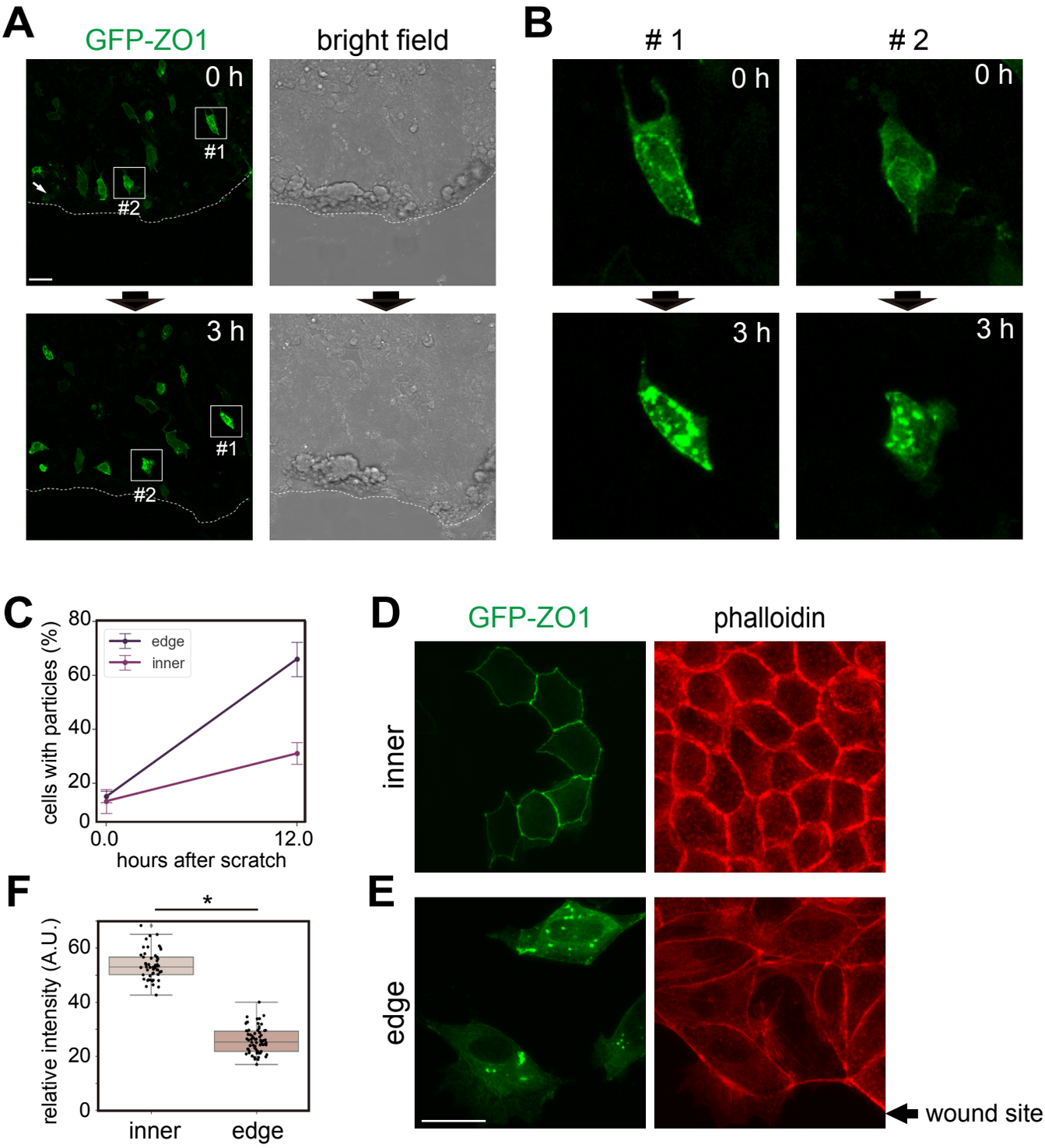

Kinoshita et al. Figure S1

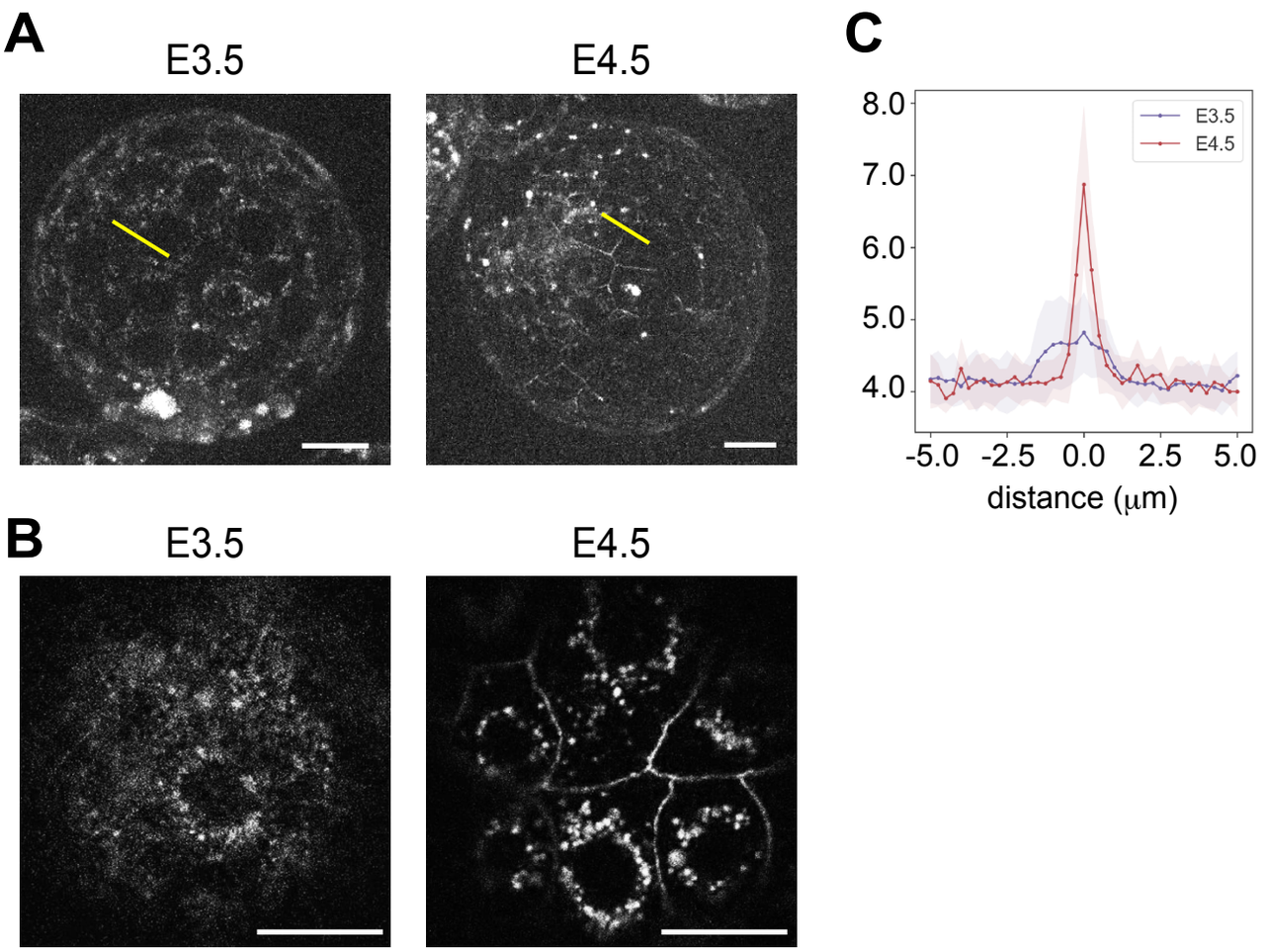

Kinoshita et al. Figure S2

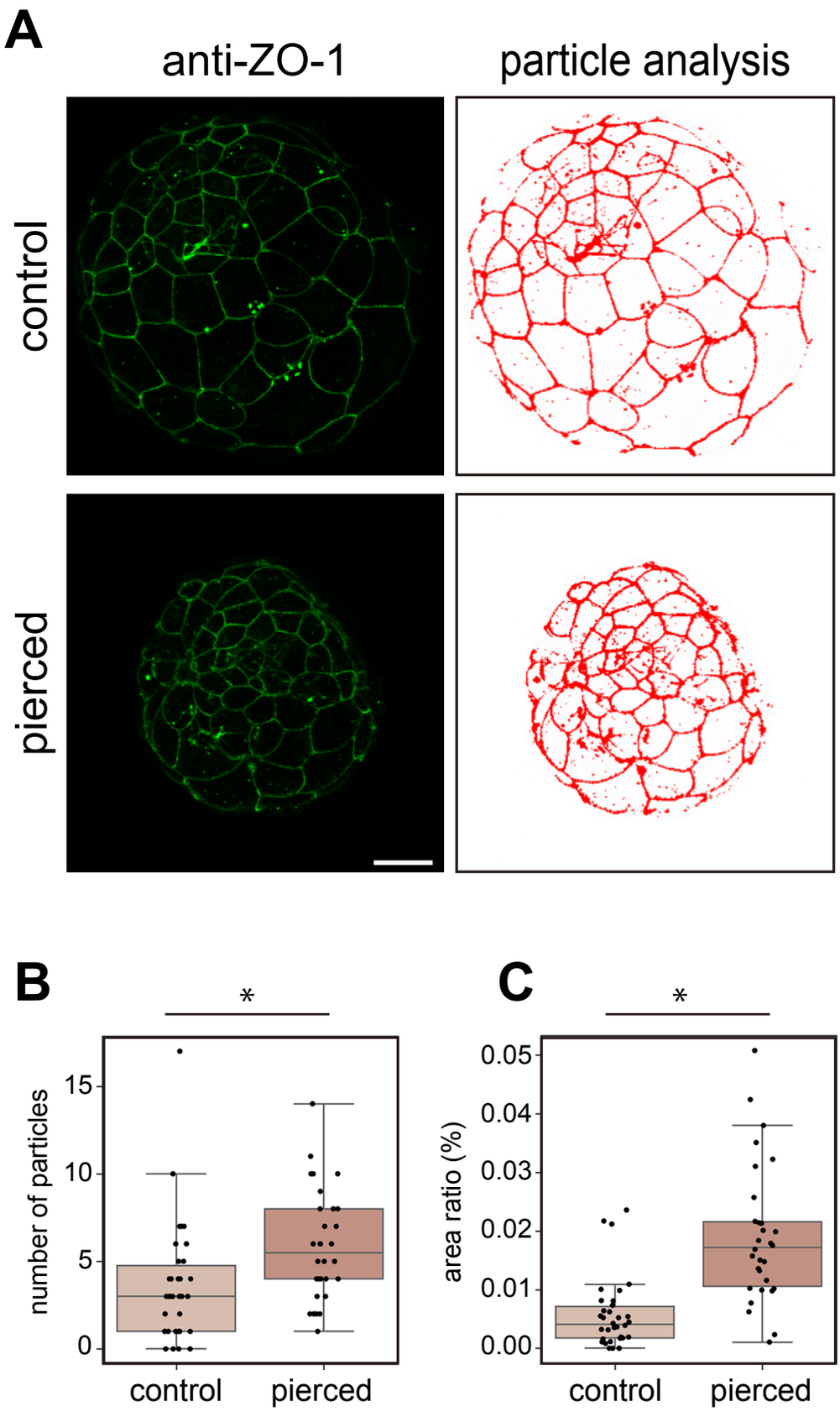

Kinoshita et al. Figure S3

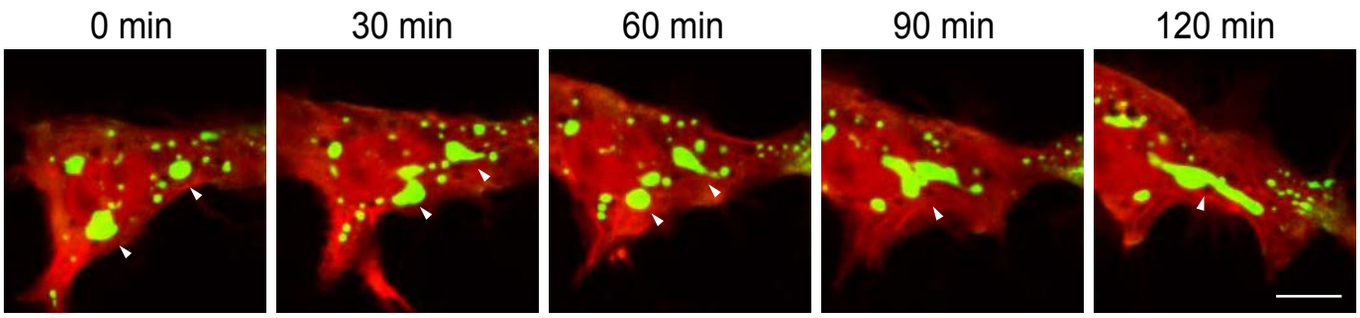

Kinoshita et al. Figure S4

trypsin-EDTA treatment

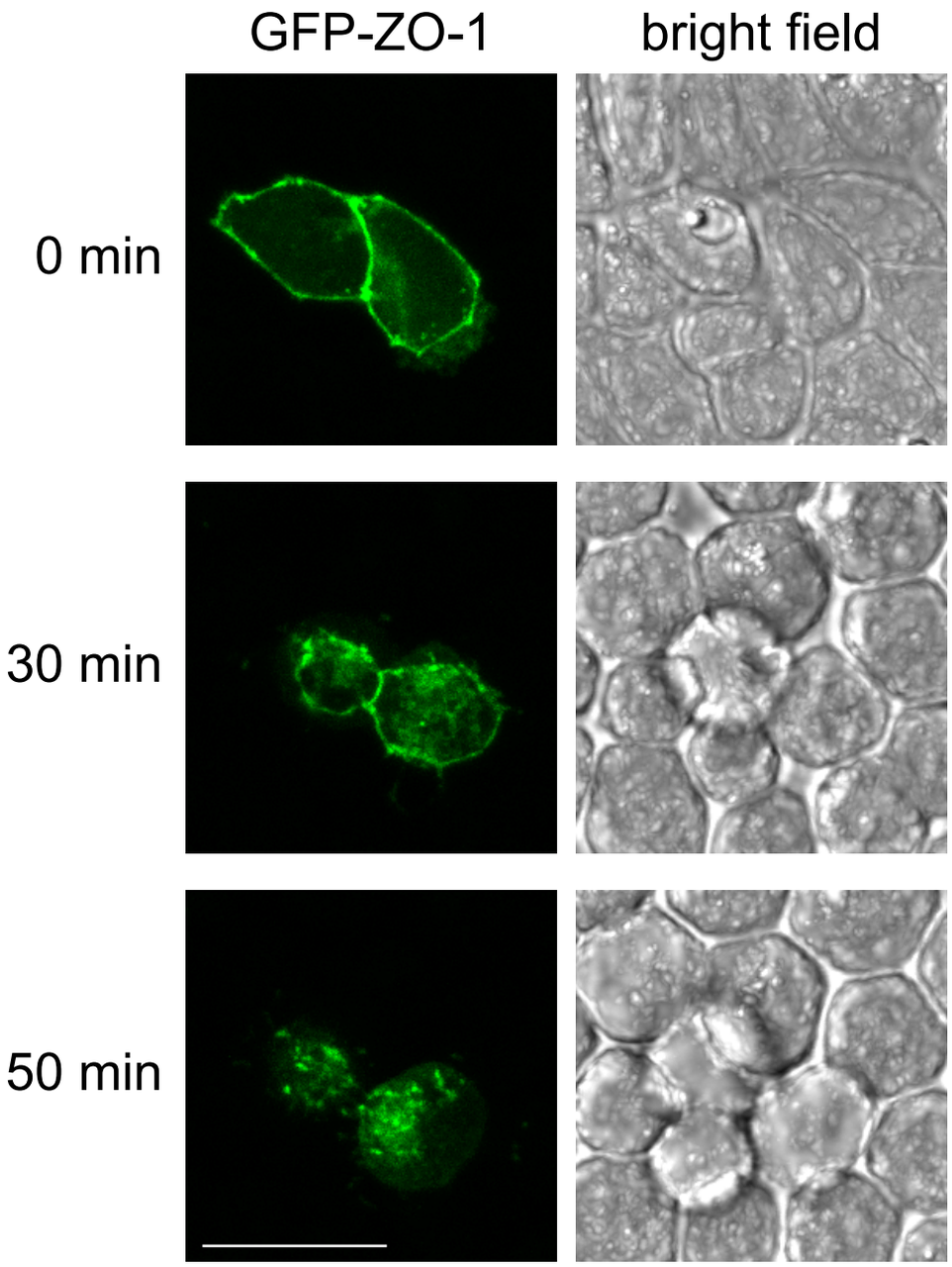
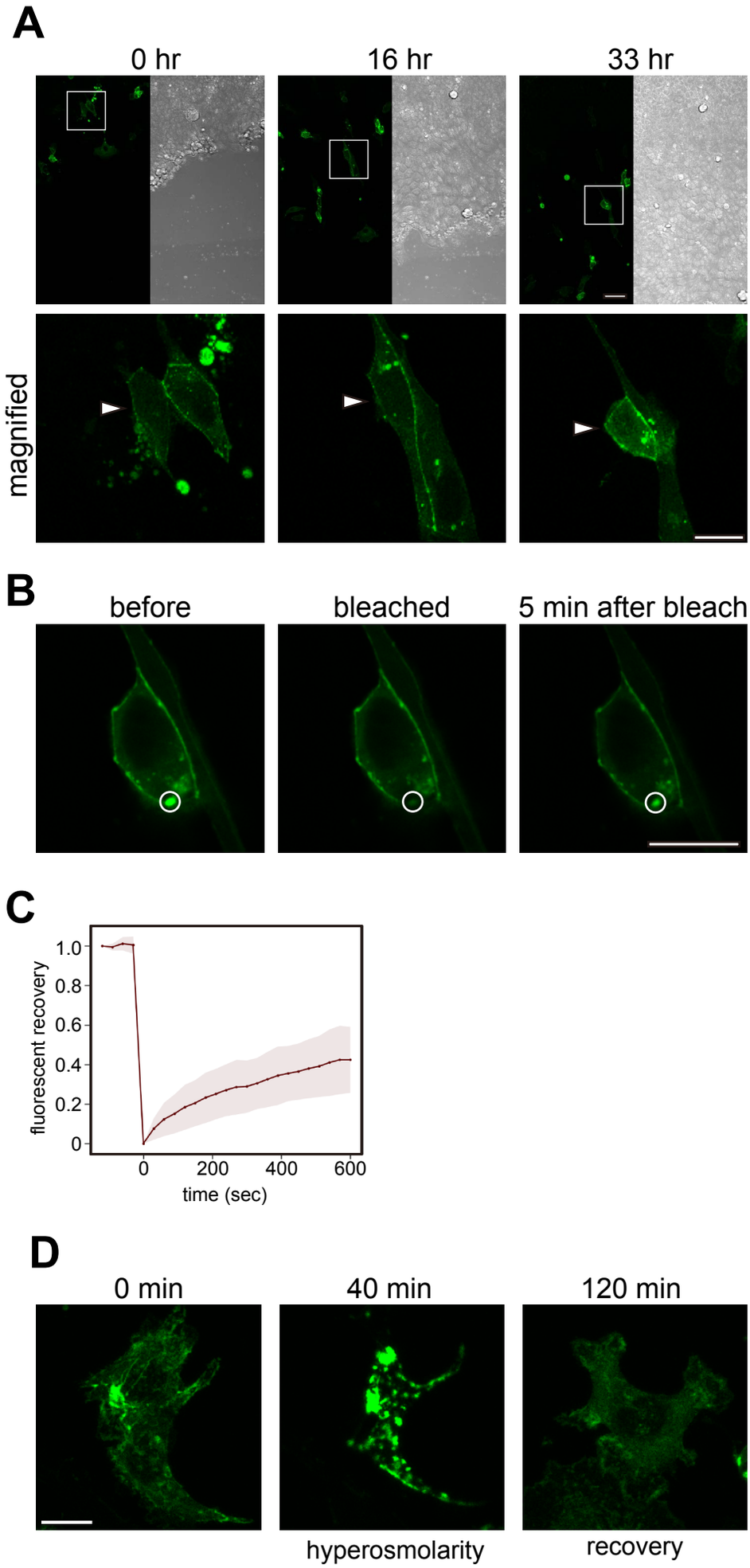
Kinoshita et al. Figure S5